

CrystEngComm

Accepted Manuscript



This is an *Accepted Manuscript*, which has been through the Royal Society of Chemistry peer review process and has been accepted for publication.

Accepted Manuscripts are published online shortly after acceptance, before technical editing, formatting and proof reading. Using this free service, authors can make their results available to the community, in citable form, before we publish the edited article. We will replace this *Accepted Manuscript* with the edited and formatted *Advance Article* as soon as it is available.

You can find more information about *Accepted Manuscripts* in the [Information for Authors](#).

Please note that technical editing may introduce minor changes to the text and/or graphics, which may alter content. The journal's standard [Terms & Conditions](#) and the [Ethical guidelines](#) still apply. In no event shall the Royal Society of Chemistry be held responsible for any errors or omissions in this *Accepted Manuscript* or any consequences arising from the use of any information it contains.

ARTICLE

Crystal-to-Crystal Structural Transformation of Hydrogen-Bonding Molecular Crystals of (Imidazolium)(3-Hydroxy-2-quinoxalinecarboxylate) through H₂O Adsorption–Desorption

Cite this: DOI: 10.1039/x0xx00000x

Received 00th January 2012,
Accepted 00th January 2012

DOI: 10.1039/x0xx00000x

www.rsc.org/

Y. Yoshii,^a K. Sakai,^{*b} N. Hoshino,^{a,c} T. Takeda,^{a,c} S. Noro,^d T. Nakamura,^d and T. Akutagawa^{*a,c}

The Brønsted acid-base reaction between 3-hydroxy-2-quinoxalinecarboxylic acid (Hhqxc) and imidazole (Im) in acetone-H₂O yielded two 1:1 salts: anhydrous (HIm⁺)(hqxc⁻) (**1**) and hydrated (HIm⁺)(hqxc⁻)·(H₂O) (**2**), where HIm⁺ and hqxc⁻ are imidazolium and 3-hydroxy-2-quinoxalinecarboxylate, respectively. Single crystal X-ray structural analyses and the vibrational spectra were consistent with the lactam tautomer of the hqxc⁻ anion, which formed π -dimers in both **1** and **2**. Each π -dimer in crystal **1** was connected by intermolecular N–H...O hydrogen-bonding interactions to form a linear hqxc⁻ chain, whereas the π -dimers in crystal **2** formed an intermolecular N–H...O hydrogen-bonding zigzag chain. The HIm⁺ cations existed in the crystalline space between the hydrogen-bonding hqxc⁻ anionic chains. A reversible crystal-to-crystal structural transformation between crystals **1** and **2** was observed following H₂O adsorption–desorption, which was confirmed by powder X-ray diffraction measurements, single crystal X-ray structural analyses, and H₂O adsorption–desorption isotherms at 323 K. The structural rearrangement of the hqxc⁻ anions was achieved through changes in the intermolecular hydrogen-bonding interactions. The temperature- and frequency-dependent dielectric constants of crystal **2** revealed a dielectric peak at ~330 K owing to thermal fluctuations of H₂O molecules within the crystal.

Introduction

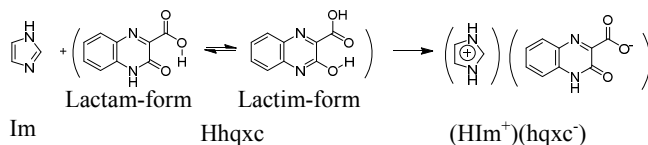
Molecular adsorption-desorption properties of metal-organic frameworks (MOFs), metal-organic coordination complexes, supramolecular organic frameworks (SOF), hydrogen-bonding porous and cage materials have been extensively examined from the viewpoints of selective gas-separation, gas-storage, and gas-transport materials.^{1–5} Such molecular adsorption-desorption processes occur in the porous crystalline environments, whose crystal structures and gas desorption properties have been characterized by the X-ray crystal structural analysis and gas adsorption-desorption isotherm. The crystal lattice of metal-organic coordination compounds can be kept before and after the molecular adsorption-desorption cycle due to relatively strong metal-ligand coordination bonds. Since the various flexible functional group can be introduced into SOF and hydrogen-bonding cage materials, dimensionality and physical functions are possibly designed. For instance, selectivity and high CO₂-adsorption ability have been reported in the proton-transferred hydrogen-bonding SOF,³ and reversible H₂O sorption up to ~20 % has been observed in organic cage molecule.^{4,5} Hydrogen-bonding one-dimensional cylinder assembly of riptycene-tris(benzimidazolone) derivative had a large BET surface area of 2796 m²g⁻¹.⁵

Dynamic behaviors of adsorption molecules in MOFs can also couple with physical responses such as ionic conducting,

magnetic, dielectric, optical properties.^{6–11} For instance, proton conducting properties of one-dimensional hydrogen-bonding imidazole chain in porous environment,^{6d} dielectric response of thermally activated molecular motions of alcohol in porous,⁷ porous spin-crossover iron(II) complex of Fe(SCN)₂(1,2-bis(4-pyridyl)-1,2-ethadiol)₂·3(C₂H₅OH) revealed a crystal-to-crystal structural transformation through C₂H₅OH adsorption into the crystals accompanying in the change of magnetic properties from the diamagnetic low-spin state to paramagnetic high-spin state.¹¹ Metal-organic Cu(I) coordination polymer also showed the crystal-to-crystal structural transformation coupled with luminescence and thermochromic behaviors through CH₃CN adsorptions-desorption.¹² The MOFs have been utilized for one of the essential structural units to design the crystal-to-crystal structural transformation through the molecular adsorption-desorption processes.¹³ On the contrary, the crystal structures of organic low-molecular weight compounds have been constructed from the intermolecular interactions such as electrostatic, hydrogen-bonding, charge-transfer, hydrophobic, van der Waals interactions, etc.,¹⁵ which magnitude was smaller than the bonding energy of metal-ligand coordination bonds. Since the crystal lattice energy of organic crystals is lower than that of MOFs, the molecular desorption–adsorption processes into the molecular crystals usually destroy the crystal lattice. Another important structural point of view is how to design the molecular adsorption crystalline space in organic crystals.¹⁶ The intrinsic pores in MOFs and porous

molecular crystals can be utilized for the molecular adsorption crystalline environments,^{13, 14} whereas there was no molecular adsorption space in the closest-packing structure of organic molecules except for the crystals including crystallization solvents and host-guest compounds.¹⁷⁻¹⁹ Therefore, the organic crystals bearing molecular adsorption – desorption properties are limited in number of the molecular structures. For instance, CO₂, CH₄, Xe, and I₂ adsorption – desorption properties in one-dimensional channel have been confirmed in porous van der Waals crystal of tris-*o*-phenylenedioxycyclotriphosphazene and bisurea macrocycles,^{17, 19} whereas H₂, CO₂, and H₂O adsorption – desorption behaviors have been observed in nonporous crystals of octylcalix[4]arene derivative and clarithromycin (6-*o*-methylerythromycin A).¹⁹ The van der Waals crystals of octylcalix[4]arene derivative captured the guest molecule weakly into the capsules, and the single crystal to single crystal phase transition has been confirmed by the inclusion of vinylbromide.¹⁹

The crystal-to-crystal structural transformation phenomena through the molecular adsorption-desorption processes are one of the interesting point of view to control the physical properties of the molecular crystals by the outer stimuli. However, typical van der Waals interactions in the molecular crystals are usually insufficient to keep the crystal lattice during the molecular adsorption-desorption cycle. Therefore, the relatively strong electrostatic and hydrogen-bonding intermolecular interactions are effective to construct the rigid molecular framework of molecular crystals. The intermolecular hydrogen-bonding networks are useful to construct the directional molecular assemblies of hydrogen-bonding capsule, chain, and, sheet,²⁰ in which the molecular adsorption-desorption environments are possible achieved. The crystalline space between the hydrogen-bonding chains and sheets can be utilized for the molecular adsorption-desorption environment.^{21, 22} The one-dimensional hydrogen-bonding chains of the organic crystals also have a potential to for the molecular adsorption-desorption environment.



Scheme 1. Molecular structures of 3-hydroxy-2-quinoxalinecarboxylic acid (Hhqxc) and imidazole (Im). Parenthesis correspond to the lactam-lactim tautomerism of Hhqxc molecule.

We notice a proton-donating π -molecule of 3-hydroxy-2-quinoxalinecarboxylic acid (Hhqxc), where the multiple hydrogen-bonding sites of –NH, C=O, and –COOH can contribute to form the intermolecular hydrogen-bonding networks (Scheme 1).²² In addition, the Hhqxc molecule shows a tautomerism between lactam-form and lactim-one according to the outer environment (Scheme 1), where the intramolecular O–H...O= hydrogen-bonding interaction formed the hydrogen-bonding sextet in both of the tautomers. Relatively high acidity has been observed in the first acid dissociation constant (pK_a) of –COOH group in Hhqxc of 2.58 in H₂O.²² Actually, Hhqxc derivatives have been utilized as a sorption material of estuarine sediment, in which the multiple hydrogen-bonding sites played an important role to adsorb the sediment.²⁴ The corresponding proton-accepting imidazole (Im) molecule was utilized for the formation of a binary molecular complex between Im and Hhqxc. Nitrogen site of Im molecule can act as the proton-accepting site with $pK_b \sim 7.0$ to form imidazolium

cation (HIm⁺).²⁵ From the pK_a values of HIm⁺ and Hhqxc molecules, the proton-transfer from Hhqxc to Im occur to form ionic molecular crystal of (HIm⁺)(hqxc⁻) during the crystal formation.²⁶ The crystal structures, H₂O adsorption-desorption properties, and dielectric responses of two (HIm⁺)(hqxc⁻) salts were examined from the viewpoint of crystal-to-crystal structural phase transition.

Experimental

Preparation of Crystals.

Commercially available Im and Hhqxc were employed for the preparations of single crystals of unhydrated (HIm⁺)(hqxc⁻) (**1**) and hydrated (HIm⁺)(hqxc⁻)·(H₂O) (**2**). Solution of imidazole (1.1 mM) and 3-hydroxy-2-quinoxalinecarboxylic acid (5.2 mmol) in acetone (9 mL) - H₂O (1 mL) was kept under the temperature controlled incubator. Slow cooling from 20 to 5 °C yielded the colorless prism-like crystals **2**. Recrystallization of **2** from C₂H₅OH yielded crystals **1**. Elemental analysis for compound **1**: Calcd for C₁₂H₁₀N₄O₃: C, 55.81; H, 3.90; N, 21.70. Found C, 55.53; H, 3.98; N, 21.57. mp 185 °C. Mixed solution of imidazole (8 mM) and 3-hydroxy-2-quinoxalinecarboxylic acid (3 mmol) in acetone (90 mL) - H₂O (10 mL) was heated under the stir, which was cooled down at 3 °C within the incubator. After 72 h, the colorless plate crystals of **2** were grown as the hydrated crystals. Elemental analysis for compound **2**: Calcd for C₁₂H₁₂N₄O₄: C, 52.17; H, 4.38; N, 20.28. Found C, 52.20; H, 4.47; N, 20.26. mp 165 °C.

Crystal Structure Determination.

Temperature-dependent crystallographic data (Table 1) were collected using a Rigaku RAPID-II diffractometer equipped with a rotating anode fitted with a multilayer confocal optic using Cu-K α ($\lambda = 1.54187$ Å) radiation from a graphite monochromator. Structure refinements were carried out using the full-matrix least-squares method on F^2 . Calculations were performed using Crystal Structure software packages.²⁷ Parameters were refined using anisotropic temperature factors except for the hydrogen atom.

Table 1. Crystal data, data collection, and reduction parameter of crystals **1** and **2**.

	1 ($T = 173$ K)	2 ($T = 100$ K)
Chemical formula	C ₁₂ H ₁₀ N ₄ O ₃	C ₁₂ H ₁₂ N ₄ O ₄
Formula weight	258.24	276.25
Space group	$P2_1/c$ (#14)	$Pbca$ (#61)
a , Å	10.4529(1)	7.02478(13)
b , Å	16.1050(2)	16.0194(3)
c , Å	7.2549(1)	21.5034(4)
β , deg	112.369(1)	
V , Å ³	1129.42(3)	2419.85(8)
Z	4	8
D_{calc} , g·cm ⁻³	1.519	1.516
μ , cm ⁻¹	9.543	9.922
Refs. meas.	12584	25159
Indep. refls.	2069	2221
Refs. used	2069	2221
R^a	0.0352	0.0422
$R_w(F^2)^a$	0.1061	0.1168
GOF	1.109	0.815

$$^a R = \frac{\sum ||F_o| - |F_c||}{\sum |F_o|} \text{ and } R_w = \frac{(\sum \omega(|F_o| - |F_c|)^2 / \sum \omega F_o^2)^{1/2}}$$

Physical measurements.

Infrared spectroscopy (Thermo Fisher Scientific Nicolet 6700) measurements were conducted with a resolution of 4 cm^{-1} using the KBr pellets. Thermogravimetry differential thermal analyses (TG-DTA) were conducted using a thermal analysis station (Rigaku Thermo plus TG8120) with Al_2O_3 as a reference in the temperature range from 293 to 600 K with a heating rate of 5 K min^{-1} under a nitrogen atmosphere. Differential scanning calorimetry (DSC) analyses were carried out by a Rigaku Thermo plus TG8120 thermal analysis station using an Al_2O_3 reference in the temperature range from 180 to 400 K with a heating rate of 5 K min^{-1} under the nitrogen. Temperature-dependent powder X-ray diffractions were collected using a Rigaku RAPID-II diffractometer equipped with a rotating anode fitted with a multilayer confocal optic using $\text{Cu-K}\alpha$ ($\lambda = 1.54187\text{ \AA}$) radiation from a graphite monochromator. Temperature-dependent dielectric constants were measured using the two-probe AC impedance method at frequencies from 1 kHz to 1 MHz (Hewlett-Packard, HP4194A) with a pellet placed into a temperature control system (Linkam, LTS350). The adsorption isotherms for H_2O at 323 K were measured with an automatic volumetric adsorption apparatus BELSORP-aqua (BEL Japan, Inc.). Before measurements, the crystals **2** were heated at 373 K under reduced pressure ($<10^{-2}\text{ Pa}$) to remove the H_2O molecules.

Results and Discussion

The pK_a and pK_b values of 3-hydroxy-2-quinoxalinecarboxylic acid (Hhqxc) and imidazole (Im) were 2.6 and 7.0, respectively.^{23, 25} The proton-transfer from proton-donor of Hhqxc to proton-acceptor of Im occurred during the crystallization according to Brønsted acid - base equilibrium. Two kinds of crystals of unhydrated ($\text{HIm}^+(\text{hqxc}^-)$) (**1**) and hydrated ($\text{HIm}^+(\text{hqxc}^-)\cdot(\text{H}_2\text{O})$) (**2**) were separately obtained from acetone- H_2O mixed solvent system according to the crystal growth condition. Since the lactam tautomer of hqxc⁻ anion was the stable molecular structure in the crystal,²³ the N-H proton of quinoxaline ring and $-\text{COO}^-$ anion were generated. The vibrational spectra in KBr pellets were also consistent with the ionic proton-transferred salts of both crystals **1** and **2**. The carbonyl stretching mode ($\nu_{\text{C=O}}$) of Hhqxc molecule was observed at 1765 cm^{-1} , whereas those of hqxc⁻ anion in crystals **1** and **2** were observed at 1672 cm^{-1} (Figure S1). The $\sim 90\text{ cm}^{-1}$ red-shift of $\nu_{\text{C=O}}$ energies in crystals **1** and **2** in contrast with that of neutral Hhqxc was consistent with the formation of $-\text{COO}^-$ anionic state. The N-H in-plane bending mode (δ_{NH}) of Hhqxc at 1630 cm^{-1} also showed $\sim 40\text{ cm}^{-1}$ red-shift at 1590 cm^{-1} of hqxc⁻ anion of crystals **1** and **2**. In the hydrated crystal **2**, the broad O-H stretching band of $\nu_{\text{OH}} = 3390\text{ cm}^{-1}$ was accordance with the existence of H_2O molecules within the crystal (Figure S1).

The crystals **1** and **2** showed a different thermal stability. The melting points of neutral Im and Hhqxc were 363 and 540 K, respectively. High thermal stability of crystal **1** up to 440 K was consistent with the formation of ionic binary salt. On the contrary, the weight-loss of $\sim 5.5\%$ at $\sim 370\text{ K}$ was observed in crystal **2**, which was consistent with the elimination of one H_2O molecule from crystal **2** (Figure S2). The H_2O elimination from crystal **2** was started around 350 K in the heating process. Although the endothermic peaks corresponding to the H_2O elimination was observed in DSC chart of the first heating process, there was an evidence for the structural phase transitions from crystals **2** to **1** (Figure S3).

Crystal structures of **1** and **2**.

The crystal structures **1** ($T = 173\text{ K}$) and **2** ($T = 100\text{ K}$) were evaluated in terms of the intermolecular hydrogen-bonding and electrostatic cation-anion interactions. The space groups of crystals **1** and **2** were the centro-symmetrical $P2_1/c$ and Pbc_a , respectively.

Figure 1 shows the molecular structures of HIm^+ cation and hqxc^- anion of crystal **1** at 173 K. The formations of HIm^+ cation and hqxc^- anion were confirmed by the existence of hydrogen atoms based on the differential Fourier map of the residual electron density. In both crystals, one HIm^+ cation and one hqxc^- anion were the crystallographically independent structural unit. Table 2 summarized the selected bond-lengths and intermolecular hydrogen-bonding distances in crystals **1** and **2**. The cationic HIm^+ structure in crystal **1** was observed by almost the equal C-N distances of N3-C12 = 1.318(3) and N4-C12 = 1.322(2) Å, and that in crystal **2** was also confirmed by almost equal N3-C12 = 1.331(2) and N4-C12 = 1.323(2) Å.²⁷ The alternate bond-lengths of C2-C3 = 1.478(3), C2-N2 = 1.295(2), and N1-C3 = 1.362(2) Å in crystal **1** were accordance with the lactam tautomer, and C3-O3 distance of 1.232(2) Å was close to the C=O double-bonding character (lactam tautomer) rather than the C-OH single bonding one (ractim tautomer).^{19a} The bond-lengths of C2-C3 = 1.482(3), C2-N2 = 1.298(2), N1-C3 = 1.359(2), and C3-O3 = 1.233(2) Å in crystal **2** was also consistent with the lactam tautomer. The torsion angle of $-\text{COO}^-$ group for the C8N2 π -plane at $119.82(15)^\circ$ in molecule **2** was almost the same to that of $122.62(16)^\circ$ in molecule **1**. The molecular conformations of **1** and **2** were almost the same to each other within the crystals **1** and **2**.

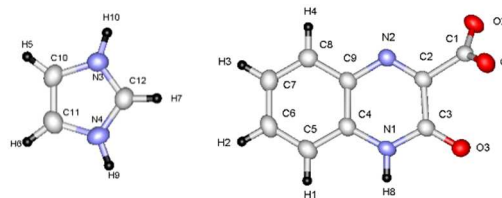


Fig. 1. Molecular structures of HIm^+ cation and hqxc^- anion in crystal **1** with thermal ellipsoids ($T = 173\text{ K}$).

Table 2. Selective bond-lengths and intermolecular hydrogen-bonding distances in crystals **1** and **2**.

	1 ($T = 173\text{ K}$)	2 ($T = 100\text{ K}$)
HIm^+		
N3-C12	1.318(3)	1.331(2)
N4-C12	1.322(2)	1.323(2)
hqxc^-		
C3-O3	1.232(2)	1.233(2)
C2-N2	1.295(2)	1.298(2)
C2-C3	1.478(3)	1.482(2)
N1-C3	1.362(2)	1.359(2)
O1-C1-C2-N2 ^a	122.62(16)	119.82(15)
Intermolecular H.B. ^b		
$\text{hqxc}^- \sim \text{hqxc}^-$	O1...H-N1 = 2.793(2)	O1...H-N1 = 2.780(2)
$\text{hqxc}^- \sim \text{HIm}^+$	O3...H-N3 = 2.808(1)	N2...H-N3 = 2.884(2)
$\text{hqxc}^- \sim \text{HIm}^+$	O2...H-N4 = 2.725(2)	O4...H-N4 = 2.670(2)

^a Dihedral angle of $-\text{COO}^-$ group of hqxc^- anion. ^b Intermolecular hydrogen-bonding interactions less than 3 Å. H. B. is hydrogen-bond.

Figure 2a show the intermolecular hydrogen-bonding unit of $(\text{hqxc}^-) \sim (\text{HIm}^+) \sim (\text{hqxc}^-)$, where the electrostatic hydrogen-bonding interactions of $\text{O2} \cdots \text{H-N4} = 2.725(2)$ and $\text{O2} \cdots \text{H-N3} = 2.808(2)$ Å connected the cation and two anions to each

other.²⁹ Figure 2b shows the unit cell of crystal **1** viewed along the *c*-axis at 100 K. Two hqxc⁻ anions formed the π -dimer with the mean interplanar distance of 3.24 Å, and the columnar arrangement of HIm⁺ cations along the *c*-axis was surrounded by the four hqxc⁻ anions within the *ab*-plane. HIm⁺ cations also formed the columnar structure along the *c*-axis, where the interplanar distances between C3N5-planes of HIm⁺ cations were 3.98 and 4.87 Å, respectively (Figure 2d). The one-dimensional linear N-H...O hydrogen-bonding (hqxc⁻)_∞ chain was observed at N1-H...O1 = 2.793(2) Å along the *c*-axis, and each hydrogen-bonding (hqxc⁻)_∞ chain was further interacted by the π -stacking interaction and electrostatic hydrogen-bonding interactions of O2...H-N3 and O2...H-N4 between the N-H proton of HIm⁺ cation and -COO⁻ group of hqxc⁻ anion. Along the *b*-axis, each hydrogen-bonding π -dimer chain was arranged at the zig-zag pattern with an angle between two π -planes of hqxc⁻ anions of 87°.

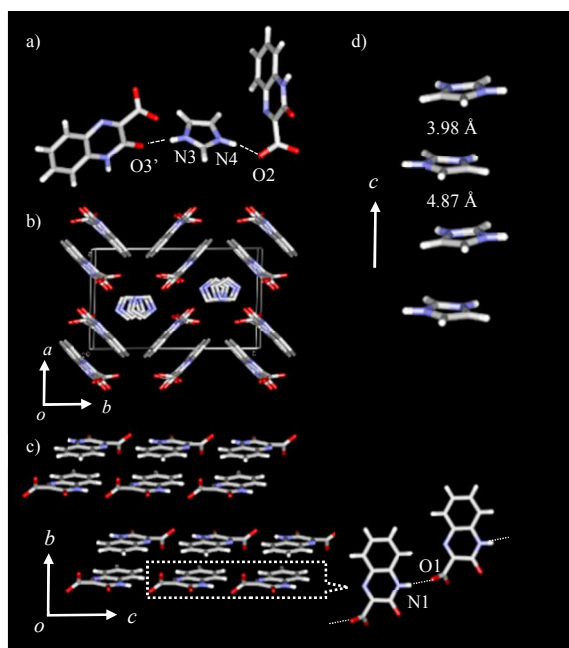


Fig. 2. Crystal structure of **1** at 173 K. a) Intermolecular hydrogen-bonding hqxc⁻ ~ HIm⁺ ~ hqxc⁻ unit. O3' is generated by symmetry operation of (x y z) = (0 0.5 -0.5). b) Unit cell viewed along the *c*-axis. c) Hydrogen-bonding π -dimer chain through the O1...H-N1 interaction along the *c*-axis. d) π -stacking column of HIm⁺ cations along the *c* axis. Mean interplanar distances between C3N2 planes were 3.98 and 4.87 Å.

The crystal structure of **2** was different from that of crystal **1** (Figure 3). One HIm⁺ cation, one hqxc⁻ anion, and one H₂O molecules were the crystallographically independent structural units. Figure 3a showed the intermolecular hydrogen-bonding hqxc⁻~HIm⁺~H₂O unit, where the effective hydrogen-bonding interactions were observed at N2...H-N3 = 2.884(2) and N4...H-O4 = 2.670(2) Å. Figure 3b indicated the unit cell of crystal **2** viewed along the *a*-axis (left and right figures were drawn by cylinder and CPK model, respectively). The alternate cation – anion arrangement was elongated along the *c*-axis. The H₂O molecules were existed the one-dimensional channel between HIm⁺ cations (right figure in Figure 3b). Figure 3c showed the hqxc⁻ anions arrangement within the *ab*-plane, where the π -stacking and hydrogen-bonding N-H...O⁻ interactions of N1-H...O1 = 2.780(2) Å connected each hqxc⁻ anions along the *a*-axis. The strength of π -dimer in crystal **2**

with the mean interplanar distance of 3.26 Å was similar to that of crystal **1** (3.24 Å). The hydrogen-bonding chain was elongated at zig-zag arrangement along the *a*-axis by the aid of the π -dimer interaction. The π -plane of HIm⁺ cations were inclined at ~54° to each other along the *a*-axis, which was different from the π -stacking structure of HIm⁺ in crystal **1**.

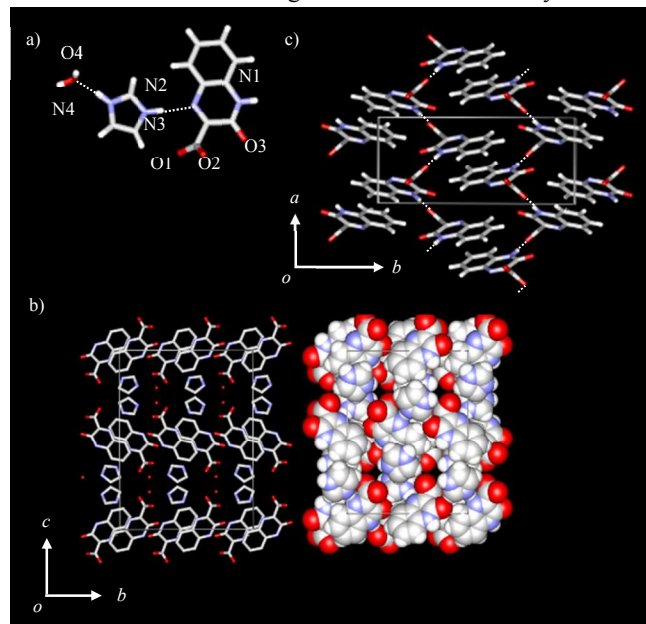


Fig. 3. Crystal structure of **2** at 100 K. a) Hydrogen-bonding structure of hqxc⁻ ~ HIm⁺ ~ H₂O. All units were crystallographically independent. b) Unit cell viewed along the *a*-axis. Right figure was CPK representation, where H₂O molecules were removed to clarify. c) Anion arrangement and intermolecular hydrogen-bonding interaction of hqxc⁻ within the *ab*-plane.

Crystal-to-crystal transformation through H₂O adsorption-desorption.

The crystals **1** and **2** were corresponded to the unhydrated and hydrated molecular assemblies, respectively, for the H₂O adsorption-desorption process. Crystal-to-crystal structural transformation through H₂O adsorption-desorption cycle was evaluated by the powder XRD measurements. The XRD patterns of crystals **1** and **2** were consistent with the simulated ones based on the single crystal X-ray crystal structural analyses. Figure 4a summarized changes in the XRD patterns for hydrated initial crystals **2** at 300 K (iii), dehydrated **2** at 373 K (iv), and H₂O re-adsorption crystals **2** (v) together with the simulated XRD patterns of crystals **1** (i) and **2** (ii). The H₂O adsorption-desorption experiments were carried out using starting crystals of hydrated crystal **2**. Firstly, the crystals **2** were hold at 373 K under the vacuum to remove the H₂O molecules, which changed the crystal color from orange to yellow (Figure 4b). The XRD pattern of dehydrated crystal **2** at 373 K (iv in Figure 4a) was consistent with that of crystal **1** (ii in Figure 4a). Therefore, the hydrated crystal **2** was transformed to the dehydrated crystal **1** through the H₂O desorption at 373 K. Since the Bragg reflections of dehydrated crystal **2** at 373 K were relatively sharp, high crystallinity was kept after the crystal transformation from crystals **2**-to-crystal **1**. The dehydrated crystals **2** at 373 K (crystal **1**) were cooling down to 300 K and kept under the saturated H₂O environment in vial during six hours, whose XRD pattern (v in Figure 4a) was consistent with that of the initial hydrated crystal **2** (iii in Figure 4a). During the H₂O adsorption process of dehydrated crystal **2**,

the yellow-color was recovered to orange ones. However, Bragg reflections of H₂O re-adsorption crystal **2** showed the slight broadening in contrast with the initial crystal **2**, suggesting the decreasing in the crystallinity through the H₂O adsorption cycle. The changes in these Bragg reflections were reversibly observed through H₂O adsorption-desorption cycle, indicating that the reversible crystal-to-crystal transformation between crystals **1** and **2** through the H₂O adsorption-desorption process.

Figure 5 shows the H₂O adsorption - desorption isotherms of crystals **2** per (HIm⁺)(hqxc⁻) unit at 323 K. Although the H₂O adsorption behavior was not confirmed in crystal **1** (Figure S5), the H₂O adsorption properties of dehydrated crystals **2** were observed in the H₂O adsorption-desorption isotherm at 323 K. The H₂O molecules of crystals **2** were previously removed by thermal treatment at 373 K under vacuum, which changed the hydrated crystal **2** to dehydrated crystal **2**. The dehydrated crystal **2** showed the same powder XRD pattern to that of crystal **1**. The unhydrated crystals **1** did not show the H₂O adsorption-desorption behavior due to the differences in the crystallite size. The crystallite sizes for **1** and **2** were observed in SEM images (Fig. S7). The dehydrated crystal **2** showed the fine crystallites to increase the adsorption surface area and induce the structural phase transition through the effective interaction with H₂O molecules. On the contrary, the relatively large size crystallites of unhydrated crystal **1** suppressed the H₂O adsorption. There was no changes in XRD profiles of **1** during adsorption-desorption isotherm (Fig. S8). The H₂O adsorption isotherm of dehydrated crystal **2** from the relative pressure (P/P_0) from 10⁻² suddenly increased the amount of H₂O adsorption around $P/P_0 \sim 0.95$, where adsorption amount n_{ads} was reached at 2.5 mol mol⁻¹ with overshooting behavior of P/P_0 . The maximum $n_{\text{ads}} \sim 2.5$ was rapidly decreased at $n_{\text{ads}} \sim 1.0$ in the H₂O desorption process from $P/P_0 \sim 0.95$ to 0.90, and saturated to a constant n_{ads} value of 1.0 at $P/P_0 \sim 0.85$. Two chemical states of $n_{\text{ads}} \sim 0$ and ~ 1 at $P/P_0 < 0.85$ were corresponded to crystals **1** and **2**.

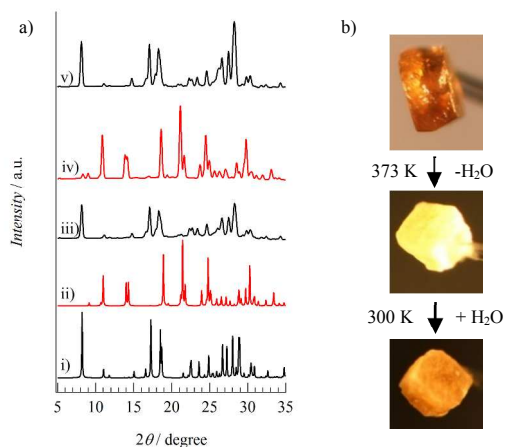


Fig. 4. Structural change of crystal **2** by the H₂O adsorption-desorption processes. a) Simulated powder XRD patterns of crystals **2** (i) and **1** (ii) based on the single crystal X-ray structural analyses. Powder XRD patterns of crystal **2** at 300 K and the peak at 8.3° was predicted for the incomplete desolvation process (iii), dehydrated crystal **2** at 373 K (iv), and re-hydrated crystal **2** at 300 K under the saturated H₂O environment during 6 h (v). b) Color changes from initial orange crystal **2**, yellow-colored dehydrated crystal **2** at 373 K, and orange-colored H₂O re-adsorption crystal **2**.

The reversible structural transformation between crystals **2** and **1** was achieved by the thermal treatments (H₂O desorption) and H₂O re-adsorption, which were consistent with the changes in the powder XRD patterns and H₂O adsorption-desorption isotherm at 323 K. Figure showed the schematic draw of the structural reconstruction from hydrated crystal **2** to crystal **1**. The hqxc⁻ anion π -dimers in crystal **2** were connected by the N-H \cdots O hydrogen-bonding zigzag chain (left in Figure 6), and there was no π -stacking interaction between HIm⁺ cations. The H₂O elimination from (H₂O) \cdots (HIm⁺) \cdots (hqxc⁻) hydrogen-bonding unit in crystal **2** resulted in the structural transformation to the linear π -dimer hydrogen-bonding chains and π -stacking columnar structure of HIm⁺ cations, where the rotations and translations of hqxc⁻ π -dimers and HIm⁺ cations were induced by the H₂O elimination process. After the H₂O elimination from crystal **2**, the angle between the π -planes of the hqxc⁻ dimers was increased from the angle of 87° in crystal **2** to 110° in crystal **1**. Since the crystal density of **1** was almost the same to that of crystal **2**, the structural reconstruction occurred with keeping in the closest-packing structure of hqxc⁻ anions and HIm⁺ cations. One of the possible reason for the difference in H₂O adsorption properties between crystals **1** and **2** is a difference in the particle size and clack formation of the crystal surface (Figure S7). Other possibility of the surface chemical property should be assumed for an exact explanation of these behaviours.

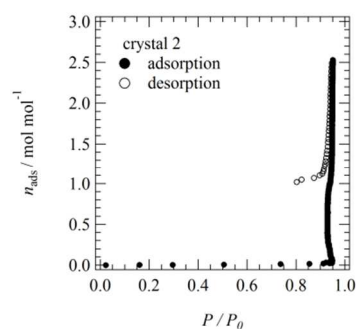


Fig. 5. The adsorption-desorption isotherms of H₂O molecule in crystal **2** at 323 K. The number of H₂O molecules per (HIm⁺)(hqxc⁻) unit (n_{ads}) vs. relative pressure (P/P_0) of H₂O molecules.

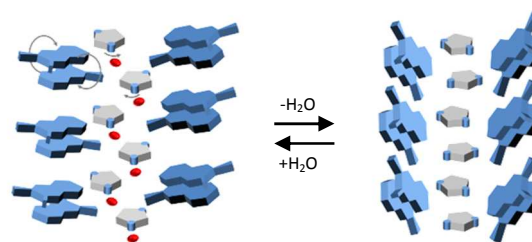


Fig. 6. Schematic representation of structural transformation in hqxc⁻ anion and HIm⁺ cation arrangements through the H₂O desorption from crystal **2** (left) to **1** (right).

Dielectric properties.

Figures 7a and 7b show the temperature- and frequency-dependent real part (ϵ_1) and imaginary part (ϵ_2) dielectric constants of the compressed pellet of crystal **2**. Although the crystal **1** did not show dielectric responses (Figure S4), both of the ϵ_1 and ϵ_2 responses were observed in hydrated crystal **2** around 330 K. Since this temperature was almost the consistent

with the H₂O adsorption – desorption temperature of 320 K, thermally activated molecular motions for the H₂O desorption process were observed in the dielectric measurements. The H₂O molecule in crystal **2** was completely removed at 380 K, where the weight-loss of ~5.5 % at 380 K was consistent with the calculated weight of one H₂O molecule (5.4 %). The weight-loss of 0.3 % at 350 K in TG chart was corresponded to the beginning of H₂O elimination from the crystal **2**, and the H₂O molecules in crystal **2** were kept within the crystal at least 330 K (Figure S2). Therefore, the dielectric ϵ_1 and ϵ_2 anomalies of crystal **2** were governed by the thermally activated molecular motion of H₂O. The ϵ_1 and ϵ_2 enhancements at 330 K were dominated by the low frequency measurements, corresponding to the slow motional freedom of H₂O molecules within the crystals. The ϵ_1 and ϵ_2 at 330 K at 1 KHz reached at 1.6 and 3.6, respectively. Before the H₂O elimination from crystal **2**, the motional freedom of H₂O molecules were thermally activated within the crystals, which also closely associated with the H₂O adsorption – desorption properties at 320 K.

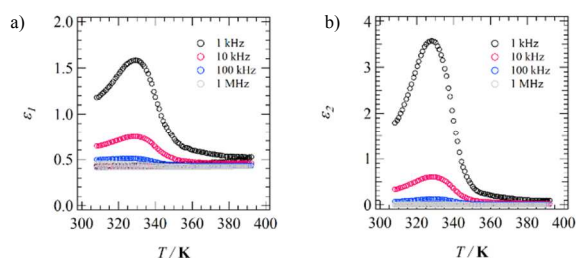


Fig. 7. Temperature- and frequency-dependent a) real part ϵ_1 and b) imaginary part ϵ_2 of compressed pellet of crystal **2**.

Conclusions

Two kinds of binary organic salts between 3-hydroxy-2-quinoxalinecarboxylate (hqxc⁻) and imidazolium (HIm⁺) were obtained as (HIm⁺)(hqxc⁻) (**1**) and hydrated (HIm⁺)(hqxc⁻)•(H₂O) (**2**). The one-dimensional hydrogen-bonding linear (hqxc⁻)_∞ and zigzag (hqxc⁻)_∞ chains were observed in crystals **1** and **2**, respectively. Each hydrogen-bonding (hqxc⁻)_∞ chain was further connected by (hqxc⁻)₂ π-dimer interaction. The crystallization H₂O molecules in crystal **2** were existed in the one-dimensional channel between (hqxc⁻)_∞ chains and HIm⁺ cations. Although the effective intermolecular hydrogen-bonding interaction between HIm⁺ and H₂O in crystal **2** stabilized the molecular orientation of H₂O within the channel, the H₂O desorption – adsorption isotherm of dehydrated crystal **2** at 320 K showed the reversible H₂O sorption properties and structural transformation of crystals **1**-to-**2**, which were further supported by the changes in powder X-ray diffraction patterns during H₂O adsorption-desorption processes. The structural transformation of hqxc⁻ anion arrangement between the N–H•••O hydrogen-bonding zigzag chain and linear chain was caused by the H₂O adsorption-desorption process. The motional freedom of polar H₂O molecules around 330 K in crystals **2** was observed in the frequency dependent dielectric responses. Such motional freedom should be essential to realize the structural transformation coupled with the H₂O adsorption-desorption properties.

Acknowledgements

This work was supported by a Grant-in-Aid for Science Research from the Ministry of Education, Culture, Sports, Science, and Technology of Japan, and by Management Expenses Grants for National Universities of Japan.

Notes and references

^a Graduate School of Engineering, Tohoku University, Sendai 980-8579, Japan.

^b Department of Bio- & Material Photonics, Chitose Institute of Science and Technology (CIST), Bibi, Chitose 066-8655, Japan.

^c Institute of Multidisciplinary Research for Advanced Materials (IMRAM), Tohoku University, 2-1-1 Katahira, Aoba-ku, Sendai 980-8577, Japan. E-mail: akuta@tagen.tohoku.ac.jp; Fax: +81 222175655

^d Research Institute for Electronic Science, Hokkaido University, Sapporo 001-0020, Japan.

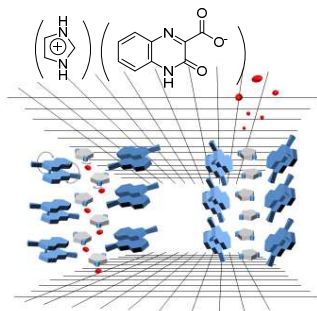
† Footnotes should appear here. These might include comments relevant to but not central to the matter under discussion, limited experimental and spectral data, and crystallographic data.

Electronic Supplementary Information (ESI) available: [The atomic numbering scheme, DSC and TG chart, vibrational spectra, UV-vis spectra, adsorption-desorption isotherms of H₂O molecule in crystal **1**, and dielectric constant of crystal **1**.] See DOI: 10.1039/b000000x/

- (a) S. Kitagawa, R. Kitaura, S. Noro, *Angew. Chem. Int. Ed.* 2004, **43**, 2334; (b) J. C. L. Rowsell, O. M. Yaghi, *Micro. Meso. Mater.* 2004, **73**, 3; (c) D. Dymtsev, H. Chun S. H. Yoon D. Kim. K. Kim, *J. Am. Chem. Soc.* 2004, **126**, 32; (d) M. Dinca, J. R. Long, *J. Am. Chem. Soc.* 2005, **127**, 9376; (e) B. Chen, S. Ma, F. Zapata, F. R. Fronczek, E. B. Lobkovsky, H. -C. Zhou, *Inorg. Chem.* 2007, **46**, 1233; (f) J. -R. Li, J. Ryan R. J. Kuppler, H. -C. Zhou, *Chem. Soc. Rev.*, 2009, **38**, 1477; (g) J. An, S. J. Geib, N. L. Rosi, *J. Am. Chem. Soc.* 2010, **132**, 38.
- (a) J. S. Seo, D. Whang, H. Lee, S. I. Jun, Y. J. Oh, Y. J. Jeon, K. Kim, *Nature* 2000, **404**, 982; (c) C. -D. Wu, A. Hu, L. Zhang, W. Lin, *J. Am. Chem. Soc.* 2005, **127**, 8940; (b) J. Y. Lee, O. K. Farha, J. Roberts, K. A. Scheidt, S. B. T. Nguyen, J. T. Hupp, *Chem. Soc. Rev.* 2009, **38**, 1450; (c) L. Ma, C. Abney, W. Lin, *Chem. Soc. Rev.* 2009, **38**, 1248.
- (a) J. Lü, C. Perez-Krap, M. Suyetin, N. Alsmail, Y. Yan, S. Yang, W. Lewis, E. Bichoutskaia, C. Tang, A. Blake, R. Cao, M. Schröder, *J. Am. Chem. Soc.*, 2014, **136**, 12828.
- (a) L. Chen, P. Reiss, S. Chong, D. Holden, K. Jelfs, T. Hasell, M. Little, A. Kewley, M. Briggs, A. Stephenson, K. Thomas, J. Armstrong, J. Bell, J. Busto, R. Noel, J. Liu, D. Strachan, P. Thallapally, A. Cooper, *Nat Mater*, 2014, **13**, 954; (b) T. Hasell, M. Schmidtman, C. Stone, M. Smith, A. Cooper, *Chem. Commun.* 2012, **48**, 4689.
- (a) J. Jones, T. Hasell, X. Wu, J. Bacsa, K. Jelfs, M. Schmidtman, S. Chong, D. Adams, A. Trewin, F. Schiffman, F. Cora, B. Slater, A. Steiner, G. Day, A. Cooper, *Nature*, 2011, **474**, 367; (b) M. Schneider, I. Oettel, H. Ott, L. Lechner, H. Hauswald, R. Stoll, M. Mastalerz, *Chem. Eur. J.*, 2012, **18**, 836; (c) M. Mastalerz, I. Oettel, *Angew. Chem. Int. Ed.*, 2012, **51**, 5252.
- (a) H. Kitagawa, Y. Nagao, M. Fujishima, R. Ikeda, S. Kanda, *Inorg. Chem. Commun.* 2003, **6**, 346; (b) M. Sadakiyo, T. Yamada, H. Kitagawa, *J. Am. Chem. Soc.* 2009, **131**, 9906; (c) J. M. Taylor, R. K. Mah, I. L. Moudrakovski, C. I. Ratcliffe, R. Vaidhyanathan, G. K. H. Shimizu, *J. Am. Chem. Soc.* 2010, **132**, 14055; (d) S. Bureekaew, S. Horike, M. Higuchi, M. Mizuno, T. Kawamura, D. Tanaka, N. Yanai, S. Kitagawa, *Nat. Mater.* 2009, **8**, 831.
- K. Barthelet, J. Marrot, D. Riou, G. Féry, *Angew. Chem. Int. Ed.* 2002, **114**, 291.
- (a) W. Zhang, Y. Cai, R. -G. Xiong, H. Yoshikawa, K. Awaga, *Angew. Chem. Int. Ed.* 2010, **49**, 6608; (b) S. Frunza, A. Schönhals, L. Frunza, P. Ganea, H. Kosslick, J. Harloff, A. Schulz, *J. Phys. Chem. B* 2010, **114**, 12840; (c) S. Devautour-Vinot, G. Maurin, C. Serre, P. Horcajada, D. P. da Cunha, V. Guillerme, E. de S. Costa, F. Taulelle, C. Martineau, *Chem. Mater.* 2012, **24**, 2168.
- M. D. Allendorf, C. A. Bauer, R. K. Bhakta, R. J. T. Houk, *Chem. Soc. Rev.*, 2009, **38**, 1330.

- 10 (a) H. –B. Cui, K. Takahashi, Y. Okano, H. Kobayashi, Z. Wang, A. Kobayashi, *Angew. Chem. Int. Ed.* 2005, **44**, 6508; (b) H. –B. Cui, Z. Wang, K. Takahashi, Y. Okano, H. Kobayashi, A. Kobayashi, *J. Am. Chem. Soc.* 2006, **128**, 15074.
- 11 S. M. Neville, G. J. Halder, K. W. Chapman, M. B. Duriska, P. D. Southon, J. D. Cashion, J. –F. Létard, B. Moubaraki, K. S. Murray, C. J. Kepert, *J. Am. Chem. Soc.* 2008, **130**, 2869.
- 12 T. H. Kim, Y. W. Shin, J. H. Jung, J. S. Kim, J. Kim, *Angew. Chem. Int. Ed.* 2008, **47**, 685.
- 13 (a) M. P. Suh, J. W. Ko, H. J. Choi, *J. Am. Chem. Soc.* 2002, **124**, 10976; (b) J. –P. Zhang, Y. –Y. Lin, W. –X. Zhang, X. –M.; Chen, *J. Am. Chem. Soc.* 2005, **127**, 14162; (c) C. Serre, S. Bourrelly, A. Vimont, N. A. Ramsahye, G. Maurin, P. L. Llewellyn, M. Daturi, Y. Filinchuk, O. Leynaud, P. Barnes, G. Férey, *Adv. Mater.* 2007, **19**, 2246; (d) S. N. Mobin, A. K. Srivastava, P. Mathur, G. K. Lahiri, *Inorg. Chem.* 2009, **48**, 4652; (e) H. –X. Li, Z. –G.; Ren, D. Liu, Y. Chen, J. –P. Lang, Z. –P. Cheng, X. –L.; Zhu, B. F. Abrahams, *Chem. Commun.* 2010, **46**, 8430; (f) K. L. Gurunatha, G. Mostafa, D. Ghoshal, T. K. Maji, *Cryst. Grow. Des.* 2010, **10**, 2483; (g) X. –D. Zheng, M. Zhang, L. Jiang, T. –B. Lu, *Dalton Trans.* 2012, **41**, 1786; (h) Y. Inokuma, S. Yoshioka, J. Ariyoshi, T. Arai, Y. Hitora, K. Takada, S. Matsunaga, K. Rissanen, M. Fujita, *Nature* 2013, **495**, 461.
- 14 (a) M. Little, M. Briggs, J. Jones, M. Schmidtman, T. Hasell, S. Chong, K. Jelfs, L. Chen, A. Cooper, *Nat. Chem.*, 2015, **7**, 153; (b) M. Mastalerz, *Angew. Chem. Int. Ed.*, 2010, **49**, 5042; (c) J. Tian, P. Thallapally, B. McGrail, *CrystEngComm*, 2012, **14**, 1909; (d) G. Zhang, M. Mastalerz, *Chem. Soc. Rev.*, 2013, **43**, 1934; (e) J. Holst, A. Trewin, A. Cooper, *Nat. Chem.*, 2010, **2**, 915; (f) G. Zhang, O. Presly, F. White, I. Oppel, M. Mastalerz, *Angew. Chem. Int. Ed.*, 2014, **53**, 1516; (g) M. Mastalerz, *Angew. Chem. Int. Ed.*, 2010, **49**, 5042; (h) G. Zhang, O. Presly, F. White, I. Oppel, M. Mastalerz, *Angew. Chem. Int. Ed.*, 2014, **53**, 5126; (i) S. Elbert, F. Rominger, M. Mastalerz, *Chem. – Eur. J.*, 2014, **20**, 16707; (j) M. Bojdys, M. Briggs, J. Jones, D. Adams, S. Chong, M. Schmidtman, A. Cooper, *J. Am. Chem. Soc.*, 2011, **133**, 16566.
- 15 A. I. Kitaigorodskii in *Molecular Crystals and Molecules*, Academic Press, London, **1973**.
- 16 (a) M. A. Garcia-Garibay, *Proc. Natl. Acad. Sci. USA* 2005, **102**, 10771; (b) T. V. Khuong, J. E. Nuñez, C. E. Godinez, M. A. Garcia-Garibay, *Acc. Chem. Res.* 2006, **39**, 413; (c) T. Akutagawa, T. Nakamura, *Dalton Trans.* 2008, 6335; (d) T. Akutagawa, H. Koshinaka, D. Sato, S. Takeda, S. Noro, H. Takahashi, R. Kumai, Y. Tokura, T. Nakamura, *Nature Mater.* 2009, **8**, 342.
- 17 (a) H. R. Allcock, M. L. Levin, R. R. Whittle, *Inorg. Chem.* 1986, **25**, 41; (b) P. Sozzani, A. Comotti, R. Shionutti, T. Meersmann, J. W. Logan, A. Pines, *Angew. Chem. Int. Ed.* 2000, **39**, 2695; (c) T. Hertzsch, F. Budde, E. Weber, J. Hullinger, *Angew. Chem. Int. Ed.* 2002, **41**, 2281; (d) P. Sozzani, S. Bracco, A. Comotti, L. Ferretti, R. Simonutti, *Angew. Chem. Int. Ed.* 2005, **44**, 1816.
- 18 (a) J. Yang, M. B. Dewal, L. S. Shimizu, *J. Am. Chem. Soc.* 2006, **128**, 8122; (b) M. B. Dewal, M. W. Lufaso, A. D. Hughes, S. A. Samuel, P. Pellechia, L. S. Shimizu, *Chem. Mater.* 2006, **18**, 4855.
- 19 (a) J. L. Atwood, L. L. Barbour, A. Jerga, B. L. Schottel, *Science* 2002, **298**, 1000; (b) J. L. Atwood, L. J. Barbour, A. Jerga, *Angew. Chem. Int. Ed.* 2004, **43**, 2948; (c) P. K. Thallapally, G. O. Lloyd, T. B. Wirsig, M. W. Bredenkamp, J. L. Atwood, L. J. Barbour, *Chem. Commun.* 2005, 5272; (d) P. K. Thallapally, L. Dobrzańska, T. R. Grnrich, R. B.; Wirsing, T. B.; Barbour, L. J.; Atwood, *Angew. Chem. Int. Ed.* 2006, **45**, 6506; (e) S. J. Dalgarno, P. K. Thallapally, L. J. Barbour, J. L. Atwood, *Chem. Soc. Rev.* 2007, **36**, 236; (f) P. K. Thallapally, P. B. McGrail, S. J. Dalgarno, J. L. Atwood, *Cryst. Grow. Des.* 2008, **8**, 2090; (g) J. Tian, P. K. Thallapally, S. J. Dalgarno, J. L. Atwood, *J. Am. Chem. Soc.* 2009, **131**, 13216.
- 20 (a) *Supramolecular Assembly via Hydrogen Bonds I and II*, (Ed.: D. N. Mingos), Springer: Berlin, 2004; (b) G. Gilli, P. Gilli in *The Nature of the Hydrogen Bond, Outline of a Comprehensive Hydrogen bond Theory*, Oxford University Press, Oxford, 2009.
- 21 (a) T. Dewa, K. Endo, Y. Aoyama, *J. Am. Chem. Soc.* 1998, **120**, 8933; (b) T. Tanaka, T. Tasaki, Y. Aoyama, *J. Am. Chem. Soc.* 2002, **124**, 12453.
- 22 (a) P. Brunet, M. Simard, J. D. Wuest, *J. Am. Chem. Soc.* 1997, **119**, 2737; (b) O. Saied, T. Maris, J. D. Wuest, *J. Am. Chem. Soc.* 2003, **125**, 14956.
- 23 (a) K. Sakai, S. Takahashi, A. Kobayashi, T. Akutagawa, T. Nakamura, M. Dosen, M. Kato, U. Nagashima, *Dalton Trans.* 2010, **39**, 1989; (b) S. Badoğlu, S. Yurdakul, *Spectrochimica Acta Part A*, 2013, **101**, 14; (c) B. Barszcz, J. Masternak, M. Hodorowicz, A. Jabłońska-Wawrzycka, *J. Therm. Anal. Calorim.* 2012, **108**, 971; (d) K. Sakai, K. Nagahara, Y. Yoshii, N. Hoshino, T. Akutagawa, *J. Phys. Chem. A* 2013, **117**, 3614.
- 24 W. D. Burgos, N. Pisutpaisal, *J. Cont. Hyd.* 2006, **84**, 107.
- 25 M. R. Grimmett in *Comprehensive Heterocyclic Chemistry*, (Eds.: A. R. Katritzky, C. W. Rees), Pergamon Press, New York, 1984, **5**, 345.
- 26 (a) T. Akutagawa, G. Saito, M. Kusunoki, K. Sakaguchi, *Bull. Chem. Soc. Jpn.* 1996, **69**, 2487; (b) G. Saito, Y. Yoshida, *Bull. Chem. Soc. Jpn.* 2007, **80**, 1.
- 27 (a) Crystal Structure: Single crystal structure analysis software, ver. 3.6, 2004. Rigaku Corporation and Molecular Structure Corporation; (b) G. M. Sheldrick, in *SHELXL97 Programs for Crystal Structure Analysis*, Universität Göttingen, Göttingen, Germany, 1998.
- 28 A. Quick, D. J. Williams, *Can. J. Chem.* 1976, **54**, 2465.
- 29 G. A. Jeffrey in *An Introduction to Hydrogen Bonding*, (Ed.: D. G. Truhlar), Oxford University Press, New York, 1997.

Graphical Abstract



Crystal-to-crystal structural transformation was observed following H₂O adsorption–desorption of hydrogen-bonding molecular crystals.